Meteorological forcing data for urban outdoor thermal comfort models from a coupled convective boundary layer and surface energy balance scheme

Article

Published Version

It is advisable to refer to the publisher's version if you intend to cite from the work. See Guidance on citing.

CrossMark

Meteorological forcing data for urban outdoor thermal comfort models from a coupled convective boundary layer and surface energy balance scheme

S. Onomura [a,*], C.S.B. Grimmond [b], F. Lindberg [a], B. Holmer [a], S. Thorsson [a]

[a] Department of Earth Sciences, University of Gothenburg, Gothenburg, Sweden
[b] Department of Meteorology, University of Reading, Reading, United Kingdom

ABSTRACT

Site-specific meteorological forcing appropriate for applications such as urban outdoor thermal comfort simulations can be obtained using a newly coupled scheme that combines a simple slab convective boundary layer (CBL) model and urban land surface model (ULSM) (here two ULSMs are considered). The former simulates daytime CBL height, air temperature and humidity, and the latter estimates urban surface energy and water balance fluxes accounting for changes in land surface cover. The coupled models are tested at a suburban site and two rural sites, one irrigated and one unirrigated grass, in Sacramento, U.S.A. All the variables modelled compare well to measurements (e.g. coefficient of determination = 0.97 and root mean square error = 1.5 °C for air temperature). The current version is applicable to daytime conditions and needs initial state conditions for the CBL model in the appropriate range to obtain the required performance. The coupled model allows routine observations from distant sites (e.g. rural, airport) to be used to predict air temperature and relative humidity in an urban area of interest. This simple model, which can be rapidly applied, could provide urban data for applications such as air quality forecasting and building energy modelling, in addition to outdoor thermal comfort.

© 2014 The Authors. Published by Elsevier B.V. This is an open access article under the CC BY-NC-ND license (http://creativecommons.org/licenses/by-nc-nd/3.0/).

* Corresponding author at: Gothenburg Urban Climate Group, Department of Earth Sciences, University of Gothenburg, Box 460, Gothenburg SE-405 20, Sweden.
E-mail address: shiho.onomura@gu.se (S. Onomura).

1. Introduction

Heat waves, such as the ones which occurred in Eastern Europe in 2010, North America and Australia in 2012, and China in 2013, are expected to have a large impact on human health, well-being and economic burden in the future (IPCC, 2012). Urban areas are particularly vulnerable to such effects given the density of urban populations and the compounding effect of the urban heat island, which will grow with increased population and greater urbanisation (McMichael et al., 2006; Pascal et al., 2006). To inform climate sensitive planning, intra-urban climate conditions at local (10^2–10^4 m, e.g. a district) and micro-scales (10^{-1}–10^3 m, e.g. a street canyon) need to be predicted for building energy applications and for estimating outdoor human thermal comfort in cities.

The thermal comfort at the neighbourhood to street level scale is chiefly influenced by urban structures. It varies greatly within short distances due to shadow patterns generated by urban surface geometry and radiative properties related to materials and urban density (Lindberg and Grimmond, 2011a). For the estimation of thermal comfort, micro-scale modelling of mean radiant temperature (T_{mrt}) is essential (Lindberg et al., 2008; Matzarakis et al., 2010). The T_{mrt}, which describes the radiant (short-wave and long-wave) heat exchange between a person and his or her surroundings, is defined as the 'uniform temperature of an imaginary enclosure in which the radiant heat transfer from the human body equals the radiant heat transfer in the actual non-uniform enclosure' (ASHRAE, 2001). It is considered to be one of the most important meteorological variables governing the human energy balance and thermal comfort outdoors, especially during clear and calm summer days (Mayer and Höppe, 1987).

Generally, in order to model T_{mrt} for the area of interest, the required meteorological variables (short-wave radiation, air temperature, and humidity) are obtained from observations or models. However, they are often not specific for the site (e.g. they are often derived from an airport), or rely on the use of long-term mean variables rather than typical sequences of conditions. When data from other areas are used (Erell and Williamson, 2006; Lindberg et al., 2013), often it is assumed that both areas are exposed to the same regional conditions and land surface effects on the meteorological variables are ignored. As a result, these local-scale land cover and land use characteristics systematically impact the accuracy of T_{mrt} calculations. If data are derived from atmospheric numerical simulation, sometimes with coupled urban land surface schemes (Miao et al., 2009; Flagg and Taylor, 2011; Loridan et al., 2013), this requires large computational cost.

Currently, only a few urban land surface models (ULSMs) are set up to rapidly calculate site-specific air temperature within or above the canopy layer (Swaid and Hoffman, 1990; Erell and Williamson, 2006; Bueno et al., 2012; Bueno et al., 2013; Stewart et al., 2013). Of these, only Bueno et al. (2013) and Stewart et al. (2013) take feedback from the land surface to the meso-scale atmosphere into account. Both use the Town Energy Balance (TEB) scheme (Masson, 2000) coupled to different boundary layer models.

In order to investigate daytime human thermal comfort in cities, simple methods to obtain more site-specific input meteorological variables need to be explored. In this study a scheme is developed to provide daytime meteorological variables representative of an urban area for a micro-scale urban radiation model to simulate T_{mrt}. A meso-scale slab convective boundary layer (CBL) model is coupled to two local-scale ULSMs (Section 2). Of interest is the ability of the combined model to simulate meteorological variables, accounting for land surface changes, using minimal computer resources (e.g. a personal computer), and simple inputs around meteorology, land surface cover, and initial state conditions. The number of meteorological inputs is reduced compared to those required for the separate models included in the coupled scheme. The coupled models are tested at three sites (suburban, irrigated sod-farm and unirrigated grassland) in Sacramento, CA (Sections 3 and 4). They replicate well the local-scale urban meteorological variables (air temperature and relative humidity) from those measured at rural sites (Section 6). Here the focus application is to obtain T_{mrt}, one of most critical components of outdoor human comfort, by calculation with a micro-scale urban radiation model – the SOlar and Long Wave Environmental Irradiance Geometry model (SOLWEIG) (Lindberg et al., 2008; Lindberg and Grimmond, 2011b). SOLWEIG determines three-dimensional radiation fluxes

and T_{mrt}. To ensure that the coupled model can provide robust input for this application, sensitivity tests are undertaken with SOLWEIG (Section 5.1 and 6). The coupled model scheme developed is applicable to urban climate sensitive planning issues such as the effect of land cover changes on intra urban temperature variations; building energy applications; air quality forecasting; and dispersion modelling.

2. The convective boundary layer and urban land surface models

The convective boundary layer (CBL) is strongly influenced by daytime momentum, heat, moisture and air pollutant exchanges in the urban environment. The depth of this mixing layer determines the volume for dilution of heat, water, carbon, and other atmospheric pollutants and their dispersion downwind of the city. The CBL is capped at its top by a temperature inversion and an entrainment zone (Fig. 1). Here, a simple approach to derive the growth of the CBL, the so-called "slab" model based on thermodynamic processes is used. The rate of change of air temperature and humidity within the CBL are determined from the turbulent heat fluxes and the net fluxes from the entrainment zone (Raupach, 2000). Formulated at the meso-scale (10^3–10^5 m), the slab model determines the height of the CBL (z_i), potential temperature (θ), and specific humidity (q) through time (t), using the conservation equations of heat and water vapour (e.g. Cleugh and Grimmond, 2001):

$$\frac{\partial \theta}{\partial t} = \frac{Q_H}{\rho C_p z_i} + \frac{\theta_+ - \theta}{z_i}\left[\frac{dz_i}{dt} - \overline{w_s}\right] \tag{1}$$

$$\frac{\partial q}{\partial t} = \frac{Q_E}{\rho L_v Z_i} + \frac{q_+ - q}{z_i}\left[\frac{dz_i}{dt} - \overline{w_s}\right] \tag{2}$$

where Q_H and Q_E are turbulent sensible and latent heat fluxes at the surface, ρC_p is the heat capacity of air, L_v is the latent heat of vaporization, θ_+ and q_+ are the potential temperature and specific humidity just above z_i, and w_s is the subsidence velocity of air. The rate of change of θ and q within the CBL is derived from temporally integrating the conservation equations. The CBL changes its height, z_i, in response to changes in surface heat fluxes and entrainment across the capping inversion at the top of the CBL. A number of different encroachment and entrainment schemes exist (e.g. Tennekes,
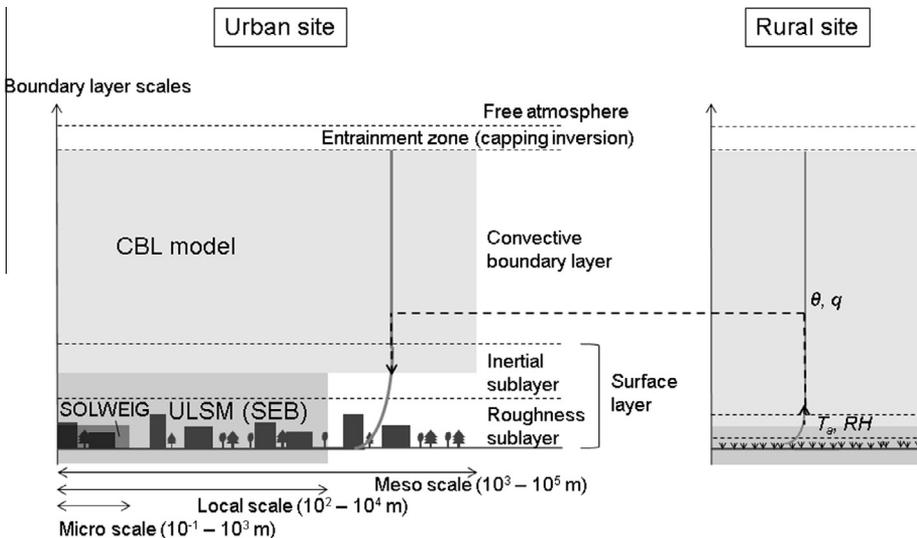

Fig. 1. Relation between boundary layer scales, the models and observations in this study: the convective boundary layer (CBL), surface energy balance (SEB) and micro-scale radiation environment (SOLWEIG), urban land surface model (ULSM).

1973; Tennekes and Driedonks, 1981; McNaughton and Spriggs, 1986; Rayner and Watson, 1991), including Tennekes and Driedonks (1981):

$$\frac{dz_i}{dt} = \frac{b_1 w_*^3 + b_2 u_*^3}{z_i \Delta\theta_v g \theta_v^{-1}} \tag{3}$$

where b_1 and b_2 are constants, w_* and u_* convective and friction velocities, θ_v and $\Delta\theta_v$ virtual potential temperature and the temperature difference across the capping inversion.

In this study, to determine the surface fluxes Q_H and Q_E, two ULSMs are used: the Surface Urban Energy and Water balance Scheme (SUEWS) (Järvi et al., 2011) and the Large-scale Urban Meteorological Parameterization Scheme (LUMPS) (Grimmond and Oke, 2002; Loridan et al., 2010). Both calculate the urban surface energy balance (Oke, 1988):

$$Q^* + Q_F = Q_H + Q_E + \Delta Q_S \quad [\text{W m}^{-2}] \tag{4}$$

where Q^* is the net all-wave radiation, Q_F the anthropogenic heat flux, and ΔQ_S the net storage heat flux. SUEWS uses a surface resistance based Penman Monteith approach, whereas LUMPS uses the de Bruin and Holtslag (1982) simplification of Penman Monteith to calculate Q_H and Q_E. The ULSMs are local-scale models (Fig. 1) applicable to a horizontal spatial extent of the order 10^2–10^4 m. The vertical extent is from the depth where there is no net exchange of heat over the period of interest to the top of the roughness sub-layer (which is approximately the lowest atmospheric layer for meso-scale boundary layer models). Both ULSMs require land cover information and meteorological data (air temperature, air humidity, incoming short-wave radiation, wind speed, and air pressure) at the local-scale.

In this study, the models have been coupled so that the CBL model calculates θ and q using Q_H and Q_E from the ULSMs, while SUEWS and LUMPS estimate the surface heat fluxes using air temperature (T_a) and relative humidity (RH) obtained from the CBL modelled θ and q in the previous time step (Fig. 2). The combined model is forced by incoming short-wave radiation ($K\downarrow$), atmospheric pressure (P) and wind speed (u), and the need for θ (and T_a), q (and RH), Q_H and Q_E are eliminated. However, as the CBL model is for convective growth, it is limited to daytime conditions only. The entrainment schemes require initial values of θ, q, and z_i (i.e. θ_0, q_0, and z_{i0}) and the vertical gradients of θ and q ($\partial\theta/\partial z$ and $\partial q/\partial z$) allow the estimation of the net fluxes from the entrainment zone for each time step (second term on right-hand-side of Eqs. (1) and (2)). The initial data, $\partial\theta/\partial z$ and $\partial q/\partial z$ require vertical information which may be obtained from radiosonde measurements (Section 3.1), re-analysis data (e.g. ERA-interim) or model output (e.g. numerical weather prediction, NWP). Radiosonde data are generally sparse, especially so in urban areas. θ_0 and q_0 can be assessed from fixed measurements at the height of inertial sublayer. However, z_{i0}, $\partial\theta/\partial z$, and $\partial q/\partial z$ are difficult to assess as measurements at the top of z_i are needed. Therefore the parameterizations or default values of z_{i0}, $\partial\theta/\partial z$ and $\partial q/\partial z$
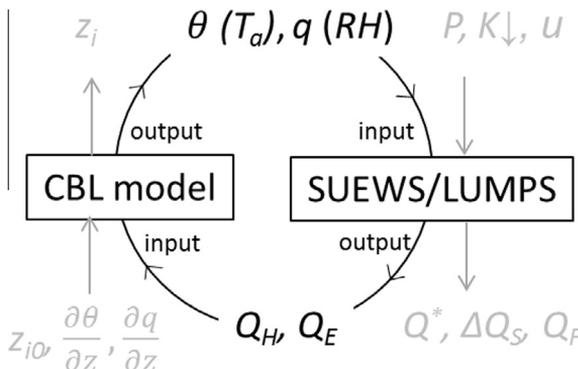

Fig. 2. Core structure with forcing input data (grey) and output (grey) from the coupled CBL model and SUEWS/LUMPS models linked via θ, q, Q_H and Q_E. For definition of notation see Appendix.

may be required to apply the coupled models in practice. To address this, we present a sensitivity test of z_{i0}, $\partial\theta/\partial z$ and $\partial q/\partial z$ (Section 5.2).

The CBL model and ULSMs potentially have different horizontal scales (Fig. 1). Here, the surface parameters for the ULSMs are assumed to be representative of the same horizontal scale as the scale of the CBL model. An alternative approach would be for the CBL model to use regionally averaged heat fluxes calculated by the ULSMs for several local-scale areas.

3. Procedures for model evaluation

3.1. Observation data

To evaluate the performance of the coupled models, meteorological data measured at a suburban site (SU) as well as dry and wet rural sites (referred to as DR and WR, respectively) in Sacramento (Fig. 3) California, U.S.A. between 20th and 29th August 1991 are used (Grimmond et al., 1993). The observation period was characterised by clear skies and warm weather. The DR area was unused and covered with tall, extremely dry grass, whereas WR was an extensive sod farm with short, irrigated grass.

At the three sites basic meteorological variables (T_a, RH, u, P, etc.), net all-wave radiation and heat fluxes were measured. The heat fluxes were determined by eddy covariance techniques. The measurement heights for each variable at each site are given in Table 1. Details of the measurement techniques and data processing are provided in Grimmond et al. (1993) and Grimmond and Oke (1995). During 22nd–24th and 26th–28th August, free flying radiosondes were released at SU (see Table I in Cleugh and Grimmond, 2001) from which initial values of $\partial\theta/\partial z$, $\partial q/\partial z$, and z_i were derived. Here z_i is defined by a potential temperature inversion. As $K\downarrow$ was not directly measured at SU, it is obtained from data produced for Sacramento Metropolitan Airport (AP), 9.3 km away, using the METSTAT solar radiation model (NREL, 2012). These data are used for all periods except for the morning of 24th August, when the METSAT $K\downarrow$ appeared to be unusually small compared to the observed Q^*, suggesting
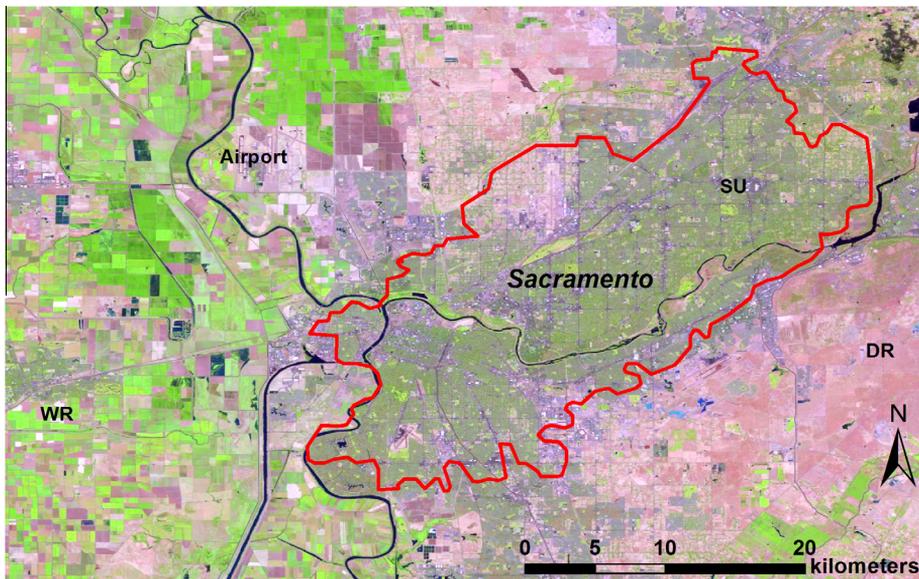

Fig. 3. Location of suburban (SU), dry rural (DR), wet rural (WR) and airport sites on a satellite image of Sacramento on 10th August 2006 (Landsat, 2006). Red line delimits the urban area. (For interpretation of the references to colour in this figure legend, the reader is referred to the web version of this article.)

Table 1
Model options and parameter values used. For definitions of notation see Appendix A.

CBL model options			
Subsidence velocity	−0.01 m s^{-1}	Entrainment scheme	Tennekes and Driedonks (1981)

	Time zone (h) −8 (to UTC)	Day light saving time & external water use (DoY)	97–300
Site-related variables	**Urban site**	**Dry site**	**Wet site**
Period (DoY)	232–241	234–241	234–241
Latitude, Longitude	38°39′N, 121°19′W	38°33′N, 121°10′W	38°31′N, 121°41′W
$A_{surface}$ (ha)	78 (a 500 m radius circle area)	10	10
Population density (in ha^{-1})	18	0	0
Land cover (plan area fraction f): (Grimmond and Oke 1999a)			
$f_{auto\ irrigation}$	0.0098	0	0
$f_{building}$	0.351	0	0
$f_{coniferous\ vegetation}$	0.064	0	0
$f_{deciduous\ vegetation}$	0.064	0	0
$f_{irrigated\ grass}$	0.349	0	1
$f_{pavement/impervious}$	0.115	0	0
f_{soil}	0.005	0	0
$f_{unirrigated\ grass}$	0	1	0
f_{water}	0.052	0	0
Roughness length for momentum: z_{0m} (m)	Macdonald et al. (1998)	0.05	0.005
Zero plane displacement: z_d (m)	Macdonald et al. (1998)	0.15	0.035
Roughness length for heat and Water vapour: z_{ov} (m)	Kawai et al. (2009)	Kawai et al. (2009)	Kawai et al. (2009)
Mean building height: z_h (m)	5.201	0	0
Mean vegetation height: z_{hv} (m)	8.369	0.5	0.05
Height of the wind speed measurement: z_m (m)[a]	9	1.8	1.3
Frontal area index: (Grimmond and Oke 1999b)			
Building	0.058	0	0
Tree	0.185	0	0

Submodel option	Urban site	Dry site	Wet site
Q^*	$L\downarrow$ is calculated by using T_a and RH Loridan et al. (2011)		

Effective surface albedo of sub-surfaces (Oke, 1987)

$\alpha_{building}$ 0.27		$\alpha_{conifer}$ 0.1	$\alpha_{deciduous}$ 0.18	α_{grass} 0.3	$\alpha_{pavement}$ 0.2	α_{water} 0.7	
Q_H, Q_E LUMPS parameters[b]		$\alpha = 0.55$	$\beta = 3$	$\alpha = 0.19$	$\beta = 3$	$\alpha = 1.0$	$\beta = 20$

Q_E SUEWS conductance air temperature limits (Järvi et al., 2011, Eq. (17))

T_H (°C)	50	T_L (°C)	0

ΔQ_s Objective hysteresis model (OHM) Grimmond et al. (1991) using the modelled Q^*

OHM coefficients	a_1	a_2	a_3			
	0.83	−0.83	−24.6	Paved[c]	$a_1 = 0.21$[d]	$a_1 = 0.35$[d]
	0.1	0.23	−6	Building[c]	$a_2 = 0.11$	$a_2 = 0.03$
	0.34	0.31	−31.4	Tree[c]	$a_3 = -16.9$	$a_3 = -26.0$
	0.32	0.54	−27.4	Grass[c]		
	0.33	0.07	−34.9	Soil[c]		
	0.50	0.21	−39.1	Water[c]		

Q_F profiles	AHDIUPRF1 and 2 (Järvi et al., 2014)	–	–

Stability function
Momentum: Unstable — Högström (1988) modified from Dyer (1974)
Stable — Van Ulden and Holtslag (1985)
Heat — Högström (1988) modified from Dyer (1974)

Initial soil stores	100 mm	1.5 mm for unirrigated grass	111 mm for irrigated grass
	(120 mm only for irrigated grass)	(0 mm for the others)	(0 mm for the others)
Initial surface stores	0 mm	0 mm	0 mm
Maximum soil moisture	150 mm	150 mm	150 mm
External water use (I_e)	Modelled by Järvi et al. (2011)	None	Observation
I_e profile	00:00 to 06:00 h 0.036		
	07:00 to 03:00 h 0.044		
	04:00 to 19:00 h 0.050		
	20:00 to 23:00 h 0.036		

[a] Air temperature, relative humidity, and air pressure were also measured at this height. The turbulent heat fluxes and all-wave radiation were measured at 29 m at SU and at the specified heights at the other two sites. Soil heat flux plates were installed at −0.068 and −0.07 m from ground surface at DR and WR sites, respectively.

[b] Note these are the effective parameters that are calculated in LUMPS.

[c] References are Anandakumar (1999) for pavement, Meyn and Oke (2009) roof, average of all seven sources in Grimmond and Oke (1999c) tree, Doll et al. (1985) grass, Fuchs and Hadas (1972) soil, Souch et al. (1998) water.

[d] See Table 2 and Section 3.2/4.

the flux may be responding to different local sky conditions. Thus for this period only, the $K\downarrow$ data are replaced by:

$$K\downarrow_{rep}(t) = Q^*(t)\overline{\left[\frac{K\downarrow}{Q^*}\right]} \tag{5}$$

using the mean diurnal relation between observed $K\downarrow$ and Q^* for the measurement period.

The soil heat flux was measured at the three sites using Campbell Scientific heat flux plates installed at 0.07 m depth with CSI TCAV temperature sensors above to account for heat divergence. Corrections are made for soil moisture content using both gravimetric and time domain reflectometry measurements.

3.2. Model settings

The complete model of the CBL provides results using SUEWS and LUMPS. For clarity we refer to these as BLUEWS (CBL model + SUEWS) and BLUMPS (CBL model + LUMPS). The model is executed according to the procedures in the manual (Järvi et al., 2014), using the options summarised in Table 1. The land cover fraction values (f) are constant for the study period.

Q^* is forced by $K\downarrow$ (Offerle et al., 2003; Loridan et al., 2010), with incoming long-wave radiation ($L\downarrow$) determined from T_a and RH. LUMPS α and β parameters for Q_H and Q_E shown in Table 1 are calculated based on the surface type. LUMPS is confirmed to have the same performance for SU as Grimmond and Oke (2002) (their Table 7). However, we found that $\beta = 20$ W m^{-2} often used for verdant vegetation is too high for DR, given the extremely dry conditions at that site. This parameter is based on observations over agricultural land (Hanna and Chang, 1992). Lower β improves the performance of LUMPS for surface heat fluxes at DR, therefore here $\beta = 3$ is used for less vegetated sites in LUMPS. ΔQ_S is calculated as a function of the modelled Q^* and surface materials based on the Objective Hysteresis Model (OHM) (Grimmond et al., 1991; Grimmond and Oke, 1999c). At SU, the OHM coefficients used are based on characteristics of the plan area surface cover (Table 1). For the rural sites, it is possible to determine the coefficients (Grimmond and Oke, 1999c) as the observed soil heat flux and net all-wave radiation data are available (Tables 1 and 2, and Section 4). Q_F for SU is estimated using the method of Järvi et al. (2011), with the same diurnal profile as determined from Vancouver data (Grimmond, 1992) (see Table 1 of Järvi et al., 2011).

The SUEWS surface resistance coefficients used are the Järvi et al. (2011) median values (50th percentile) based on a number of urban and suburban locations. The stability functions for momentum, heat and moisture used are those of Högström (1988), modified from Dyer (1974) and Van Ulden and Holtslag (1985). Roughness length for momentum (z_{0m}) and zero plane displacement length (z_d) are calculated within SUEWS for SU based on morphometric characteristics (Macdonald et al., 1998;

Table 2

Objective hysteresis model coefficients (a_1, a_2 and a_3) for unirrigated and irrigated grassed areas determined from fitting Eq. (3) in Grimmond and Oke (1999c) using observed net all-wave radiation to observed soil heat fluxes at the dry rural and wet rural sites in Sacramento. N is the number of hours of data used.

Description	Coefficients			Statistical performance				
	a_1 [–]	a_2 [s]	a_3 [W m^{-2}]	N	Slope	Intercept	R^2	*RMSE* [W m^{-2}]
Dry, long grass	0.214	0.114	−16.85	189	0.838	1.4	0.84	20.7
Short irrigated grass	0.348	0.033	−26.0	181	0.874	28.8	0.89	39.2

Grimmond and Oke, 1999b) and based on estimates using observed mean grass height (Grimmond et al., 1993) for the rural sites (Table 1). Roughness lengths for heat and water vapour are calculated based on Kawai et al. (2009).

Irrigation is regulated in Sacramento with alternating (odd/even) properties allowed to irrigate on 6 days of the week, with no irrigation permitted on Sundays (25th August) (Grimmond et al., 1993). The external water supply (or irrigation, I_e) is modelled for SU using Eq. (5) of Järvi et al. (2011) for the daily total and within day I_e profile (Table 1). The sod-farm (WR) I_e is based on the patterns observed during the fieldwork. As it has been demonstrated that urban land surface models, like their rural counterparts, need to ensure appropriate soil moisture conditions (Best and Grimmond, 2013), a spin up period of three times the study length was used. This is assumed to be most critical for SU and WR, as the natural grassland (DR) had extremely low (<2%) soil moisture, so an initial value of 1.5 mm was used. This proposed model has the advantage, compared to more complex models, that the additional computer time is insignificant, whereas for others the constraint of inadequate spin up time may need to compromise performance.

The subsidence velocity across the capping inversion of the entrainment zone for the CBL growth is set to −0.01 m s^{-1} (Cleugh and Grimmond, 2001). The Tennekes and Driedonks (1981) entrainment scheme, as recommended by Cleugh and Grimmond (2001), is used. The initial evaluation (Section 4) uses the $\partial\theta/\partial z$ and $\partial q/\partial z$ values based on the measured profiles, but during the sensitivity tests (Section 5) the effect of constant values based on the radiosonde measurements is assessed.

The model is run continuously (20th–29th August for SU; 22th–29th August for DR and WR) with the CBL model during the day and the ULSMs forced by observations at night. By using θ_0, q_0, z_{i0}, $\partial\theta/\partial z$, and $\partial q/\partial z$ (see Sections 2 and 3.1), the CBL model is initialized based on the calculated sun zenith angle (>85°) and modelled sensible heat flux (>0 W m^{-2}). All calculations are conducted using local apparent time. Initial values of θ_0 and q_0 for the rural sites use measured air temperature and humidity. For z_{i0}, $\partial\theta/\partial z$ and $\partial q/\partial z$, the SU radiosonde measurements are used for all the three sites given they are not available for the rural sites. However, these values are expected to be different at the rural sites; notably z_{i0} is expected to be lower and to differ between the rural sites. To evaluate SUEWS/LUMPS with the flux observations, a 1 h time step is needed. The ULSMs use a smaller time step (e.g. 5 min) to ensure an appropriate response relative to the water inputs (precipitation, irrigation). However, the CBL takes a longer time to adjust its properties at the meso-scale, over *ca.* 10–30 min (Cleugh and Grimmond, 2001). So the CBL calculations of z_i, θ, and q are performed at 15 min intervals using linearly interpolated data to reduce the error when the conservation equations are temporally integrated.

3.3. Model evaluation

The performance of the model, evaluated using observations from the three sites (SU, DR, and WR), is assessed without CBL feedback (referred to as SUEWS and LUMPS) and with CBL feedback (BLUEWS and BLUMPS). One code with different options selected (Järvi et al., 2014) is used with the input data and parameter settings. The focus is on Q_H and Q_E, θ and q within the CBL, and z_i for 1 h intervals during the daytime.

The statistics used for evaluation are the root mean square error (*RMSE*) and the coefficient of determination (R^2). The results for SU are also compared to Cleugh and Grimmond (2001) (referred to as CG01) model results with the same entrainment scheme (Tennekes and Driedonks, 1981).

CG01 obtained the friction velocity u_* using the logarithmic wind profile with observed u and atmospheric stability functions for momentum (same as Table 1) and roughness parameters (z_0, z_d, Grimmond and Oke, 1999b). CG01 obtained the atmospheric stability using the method given in Grimmond and Cleugh (1994). CG01 initialized CBL calculations when Q_H became positive after 05:00 and used a time step interval of 15 min for calculations.

4. Performance of the coupled model

The turbulent heat fluxes modelled using BLUEWS and BLUMPS are almost identical to those of SUEWS and LUMPS for SU and DR, differing only for Q_H at WR (Fig. 4). Almost all heat fluxes are underestimated relative to the observations during periods when these fluxes are large, while they are overestimated when fluxes are small. This trend in turbulent heat fluxes is also noted by Järvi et al. (2011). BLUEWS has a larger *RMSE* than BLUMPS for SU and WR where evaporation occurs. Larger evaporation rates are driven by stronger convective mass transfer under unstable conditions if water is available, e.g. as occurred on 22nd–24th August, compared to 26th–28th (not shown). Thus it is dependent on the surface water balance, e.g. soil moisture and external water use, which is accounted for in SUEWS but not in LUMPS. Unfortunately, there is no independent water use data to evaluate these components of the SUEWS model. However, specification of soil moisture initial conditions has been found to be important generally in ULSMs (Best and Grimmond, 2013). As the water availability for evaporation changes with the land surface characteristics, a sensitivity test is conducted (Section 5.2). The relatively large *RMSE* of SUEWS/BLUEWS Q_H results from the variance of Q_E as Q_H is calculated as the residual of the surface energy balance. Järvi et al. (2011), who found this same trend in SUEWS, noted the Q_E variance is acceptable compared to the original model of Grimmond and Oke (1991) since SUEWS reduces the input data so much. For the DR site (Fig. 4e–h), both BLUEWS and BLUMPS model
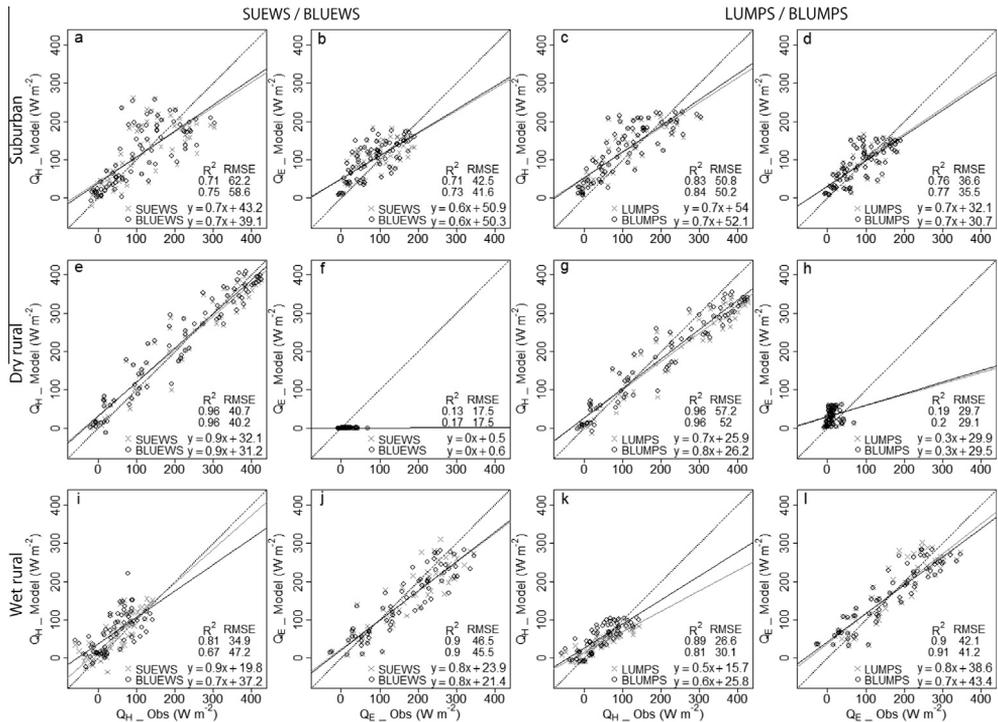

Fig. 4. Modelled sensible and latent fluxes (Q_H, Q_E) (1 h) versus the observations for uncoupled (LUMPS, SUEWS, grey) and coupled (BLUMPS, BLUEWS, black) runs for (a–d) suburban (e–h) dry rural and (i–l) wet rural. Model statistics (R^2, *RMSE*, linear regression) are shown.

Q_H well, while BLUEWS underestimates and BLUMPS overestimates Q_E. The extreme environment of DR results in excessively high surface resistance values in SUEWS/BLUEWS, and thus almost no evapo-transpiration occurs (observed values less than 70 W m^{-2}). However, since the rate of Q_E at DR is very small, it has a very small impact on the modelling of Q_H and ΔQ_S. For the WR site (Fig. 4i–l), both runs have good performance for Q_E, but the coupled Q_H results are poorer than the uncoupled results. The OHM coefficients used for modelling ΔQ_S at the rural sites are calculated using regression analysis for the observed ΔQ_S and Q^*. The performance of the modelled ΔQ_S using these coefficients and the observed Q^* compared to the observations are R^2 = 0.84 and 0.88, but $RMSE$ = 20.7 and 39.2 W m^{-2} for DR and WR, respectively (Table 2).

When the modelled z_i, θ and q within the CBL at SU are compared to the radiosonde observations and the CG01 CBL results, all runs show good overall performance (Fig. 5). The performance of the coupled runs is good for z_i and θ (R^2 and $RMSE$), but it is poorer for q. The complex observed q profiles (e.g. for August 24th, see Fig. 8 in CG01) are almost impossible for a simple slab model to predict. Given that BLU-EWS performs better than BLUMPS for q (R^2 = 0.61, $RMSE$ = 1 g kg^{-1}; R^2 = 0.48, $RMSE$ = 1.2 g kg^{-1}, respectively), the results support the use of the biophysical evaporation model SUEWS.

As expected, at DR larger growth of z_i and θ and decreasing q (Fig. 6) compared to SU are modelled (Fig. 5), while smaller growth of z_i and θ and increasing q at WR are predicted. The BLUMPS q is much larger than that derived from BLUEWS because Q_E is overestimated (underestimated) by BLUMPS (BLUEWS) (Fig. 4).

5. Sensitivity tests

Three sensitivity tests are conducted here. First, given an intended application of the coupled model is to force the micro-scale urban radiation model SOLWEIG (Lindberg et al., 2008; Lindberg and Grimmond, 2011a), we assess the impact of T_a and RH on SOLWEIG modelled T_{mrt}. Second, as the land cover characteristics influence all the surface energy balance fluxes, the changes in land cover
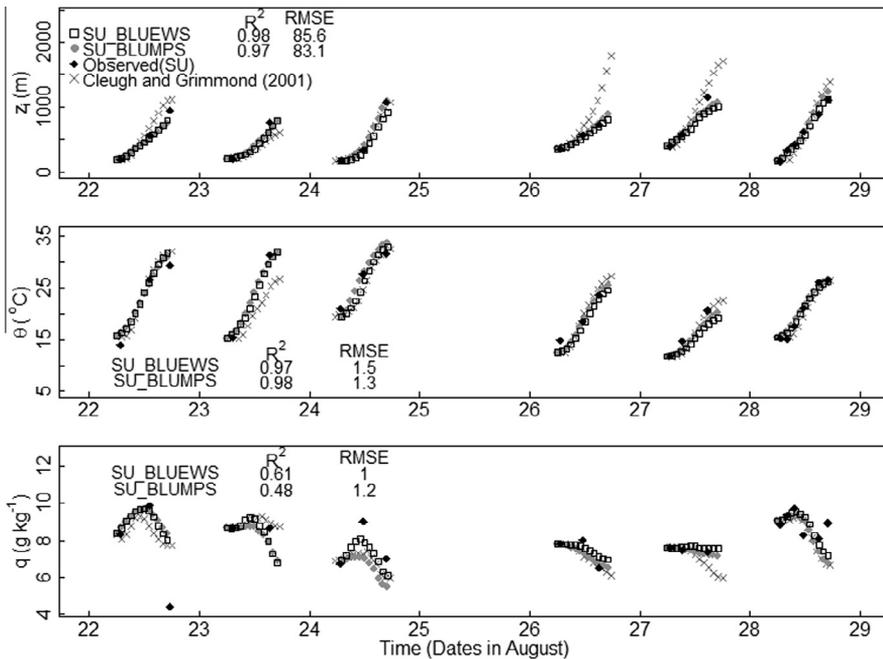

Fig. 5. Modelled convective boundary layer height (z_i), potential temperature (θ) and specific humidity (q) during 22nd–28th in August 1991 using the coupled runs (BLUEWS, BLUMPS) for suburban Sacramento with the Cleugh and Grimmond (2001) results and the radiosonde observations also shown. Modelled results plotted hourly.
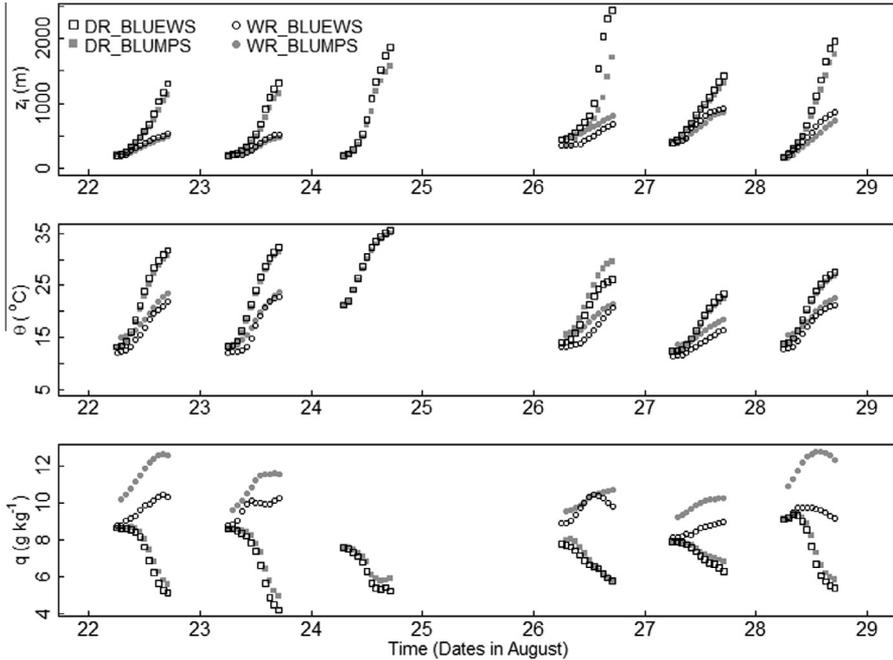
Fig. 6. Hourly modelled convective boundary layer height (z_i), potential temperature (θ) and specific humidity (q) using the coupled runs (BLUEWS, BLUMPS) for dry rural and wet rural sites (DR, WR) in Sacramento. Wet rural is not modelled on 24th August as the forcing data are missing due to irrigation.

and height of the roughness elements are explored. Third, as the coupled runs require the not easily obtained (Section 2) initial values of z_{i0}, $\partial\theta/\partial z$ and $\partial q/\partial z$ (Eqs. (1) and (2)) as forcing data for the CBL model, the parameterizations or default values may be required to apply the coupled models in practice. The impact of the alternative options on the modelled T_a and RH are explored.

5.1. SOLWEIG

SOLWEIG is run for the period 11:00–14:00 local apparent time with a standing person whose centre of gravity is at a height of 1.1 m (this equates to an 'average' person of 1.80 m height and 75 kg weight), located within a simple canyon with a sky view factor of 0.6.

For the base run (S0), observed T_a, RH, and $K\downarrow$ are compared to changes to the observed values of T_a ± 10 °C (S1) and RH ± 20% (S2) (Table 3a). Changes in calculated mean radiant temperature (ΔT_{mrt}) indicate the model is more sensitive to T_a than RH (Fig. 7). Therefore for simplicity, the variations of RH associated with the changes of T_a are ignored. The change in ΔT_{mrt} for T_a is nearly linear, with a 1 °C error in T_a producing a 0.84 °C impact on T_{mrt}. This is equal to the effect caused by about a 28% error in RH. Considering the small RH impact on T_{mrt} compared to T_a, the temperature dependency of RH is ignored in this analysis. Thus, good estimation of T_a is more critical to accurately estimate T_{mrt} than good estimate of RH (i.e. q).

5.2. SUEWS land cover characteristics

Section 4 shows that SUEWS modelled Q_F is sensitive to land surface characteristics. To examine the influence of land cover changes, sensitivity tests are performed, which include shifting land cover fractions between buildings and deciduous trees (termed SW1 in Table 3b), as well as shifting between unirrigated grass and impervious surface (SW2). Additionally, the impact of the heights of buildings and trees (SW3 and SW4) are compared. For the reference run (SW0, presented in Section 4), 50%

Table 3

Sensitivity tests to evaluate the impact on model performance of (a) SOLWEIG (period 11:00–14:00 h), (b) SUEWS (whole period), and (c) BLUEWS (daytime). Section 5 provides more details. Appendix A has notation defined. Data used: observed (ob), replaced with radiosonde data at convective boundary layer height (ra), and mean of the observations (av).

| Run code			
(a)		Variables	
SOLWEIG	$T(°C)$	$RH(\%)$	$K\downarrow(W\,m^{-2})$
S0	ob	ob	ob
S1	±10 of ob, 2 °C step	ob	ob
S2	ob	±20 of ob, 2% step	ob
(b)		Land surface characteristics	
SUEWS			
SW0		Average surface characteristics (Table 1)	
SW1		Change land cover: building to deciduous trees (±15%, 5% step)	
SW2		Change land cover: irrigated grass to pavement (±15%, 5% step)	
SW3		Change height: building (±5 m, 0.5 m step)	
SW4		Change height: tree (±5 m, 0.5 m step)	
(c)		Variables	
BLUEWS	$z_{i0}(m)$	$\partial\theta/\partial z(K\,m^{-1})$	$\partial q/\partial z(g\,kg^{-1}\,m^{-1})$
B0	ob	ob + ra	ob + ra
B1	ob	ob	ob
B2	av	av	av
B3	100–400, 25 step	av	av
B4	100, 250, 400	0.005–0.09, 0.005 step	−0.02 to 0.09, 0.01 step
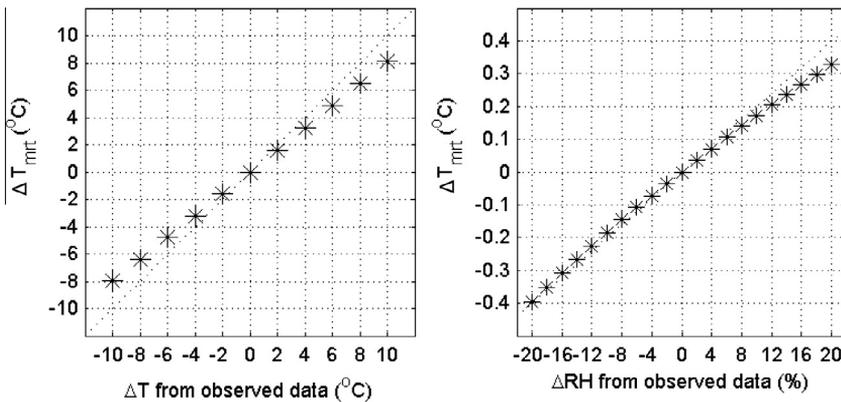
Fig. 7. Change in calculated mean radiant temperature (T_{mrt}) for the S0 run to changes in (left) air temperature (T_a) (S1) and (right) relative humidity (RH) (S2) (see Table 3a and Section 5.1).

of the 60 min modelled Q_E have absolute errors (AE$_{50}$) of less than 8.0 W m^{-2} (Fig. 8). When the fraction of deciduous trees increases by 15% (from buildings), the AE$_{50}$ increases to 10.7 W m^{-2} (Fig. 8a). Enhancing the irrigated grass by 15% (from pavement) results in AE$_{50}$ increasing to 11.2 W m^{-2} (Fig. 8b). With taller (+5 m) buildings and trees, AE$_{50}$ is 9.7 and 9.0 W m^{-2}, respectively (Fig. 8c and d). Taller buildings and trees increase z_0 and z_d, influencing convective transfers. These impacts are smaller than changes in the grass fraction, as larger grass fraction (from pavement) expands the water availability for evaporation, which impacts the modelled Q_E.

The land cover changes influence the maximum (absolute) errors (Fig. 8). The AE$_{90}$ (90% of the 60 min modelled Q_E have absolute errors) are less than 54.9 W m^{-2} on average, whereas AE$_{90}$ is largest

when grass is increased by 15% (83.1 W m^{-2}) and most improved (AE$_{90}$ = 50.5 W m^{-2}) when building height is increased by 4 m (Fig. 8). These results are also consistent with analysis of the modelled results by wind direction with hourly source area (Cleugh and Grimmond, 2001) derived land cover characteristics (not shown). This suggests that the source area shape is incorrect in some conditions.

5.3. CBL forcing data

Sensitivity tests are performed to evaluate the impact of using alternatives to z_{i0}, $\partial\theta/\partial z$ and $\partial q/\partial z$ on T_a and RH modelled by BLUEWS (Table 3). The reference analysis (termed B0 in Table 3c, and presented in Section 4) uses the observed values of z_{i0}, $\partial\theta/\partial z$ and $\partial q/\partial z$ given at sunrise and considers the change of $\partial\theta/\partial z$ and $\partial q/\partial z$ with estimated z_i at every time step. Thus $\partial\theta/\partial z$ and $\partial q/\partial z$ are replaced with the radiosonde values measured at the height of z_i at sunrise. B1 does not consider the change; z_{i0}, $\partial\theta/\partial z$ and $\partial q/\partial z$ are given by the observation at sunrise and are used consistently for all that day. B2 uses the average of initial values observed for the 6 days; these are z_{i0} = 241.5 m, $\partial\theta/\partial z$ = 0.043 K m^{-1} and $\partial q/\partial z$ = 0.009 g kg^{-1} m^{-1}. Thus, the model runs B0 to B2 become more independent of the radiosonde measurements. For these three cases (B0, B1, and B2), BLUEWS, BLUMPS and the uncoupled CBL model are run with all other model settings the same as used in Section 4.

In general, B1 and B2 have larger *RMSE* and smaller R^2 for all variables than B0 (Fig. 9). The larger error in B1, when radiosonde profile data are unavailable to adjust $\partial\theta/\partial z$ and $\partial q/\partial z$ at z_i at each time step, indicates these adjustments improve model performance. The B2 results have a smaller *RMSE* and larger R^2 for all variables compared to B1. This supports the use of typical values based on boundary layer measurements. Overall, BLUEWS and BLUMPS have similar performance to the CG01 CBL model, despite slightly poorer performance for heat fluxes for BLUEWS than BLUMPS. For BLUEWS humidity is better correlated with observations (Section 4). Only BLUEWS is assessed in the following
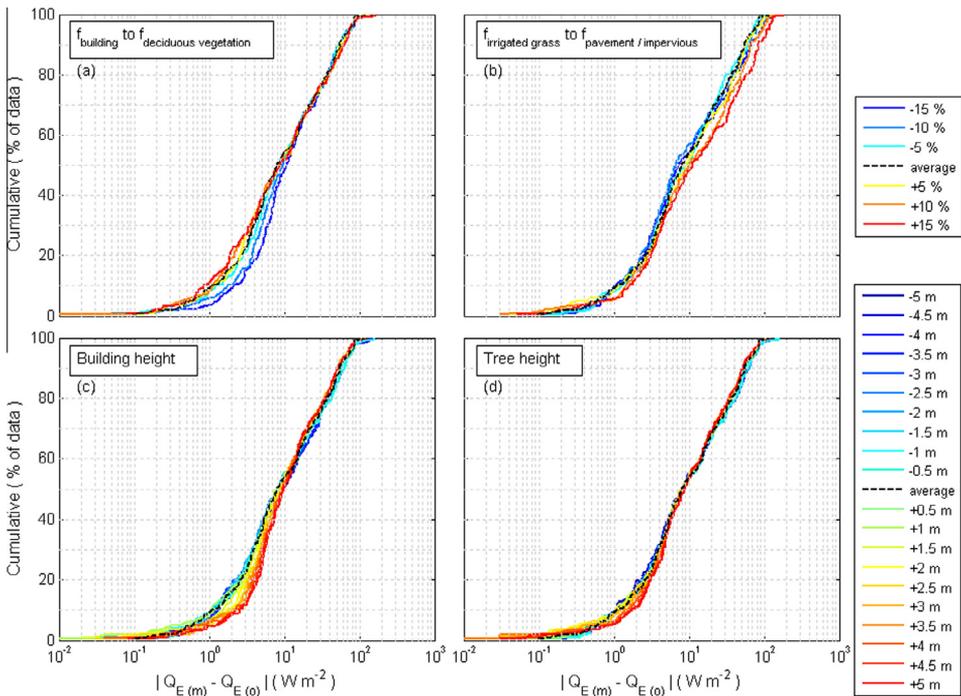

Fig. 8. Impact of changes in surface land cover characteristics on 60 min absolute latent heat flux errors (modelled (m) – observed (o)) cumulative (percent of data) for land cover changes from (a) buildings to deciduous trees, (b) irrigated grass to pavement, (c) building height, and (d) tree height. See key for range of changes used. Dash-line is average used in Section 4.
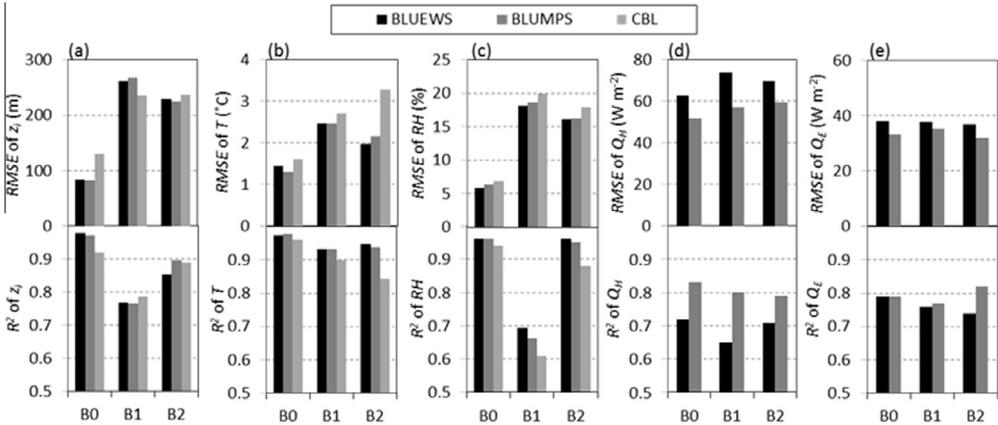
Fig. 9. Impact (Table 3c) of initial convective boundary layer (z_{i0}), vertical gradients of potential temperature and specific humidity $(\partial\theta/\partial z, \partial q/\partial z)$ on modelled (a) convective boundary layer height (z_i), (b) air temperature (T_a), (c) relative humidity (RH), (d) sensible heat flux (Q_H), and (e) latent heat flux (Q_E). Root mean square error (RMSE) (top row) and coefficient of determination (R^2) (lower row) are shown.

sensitivity tests. BLUEWS has a stronger biophysical base, so it responds to changes in surface water state, which provides the potential for the application of the coupled model system to a wide range of cities and surface water conditions.

The impact of z_{i0} on the modelled T_a and RH is tested with z_{i0} varied from 100 to 400 m in 25 m increment steps (Table 3c, B3). The RMSE of T_a and RH change from 1.4 to 2.8 °C (minimum when z_{i0} = 200 m) and 5.5% to 7.0% (minimum z_{i0} = 150 m), respectively (Fig. 10). The impact of z_{i0} is relatively small on T_a and small enough to ignore on RH. Values of z_{i0} in the range of 100–400 m are probably appropriate and supported by measurements. A mean z_{i0} of around 200 m is observed during autumn under clear sky conditions by Doppler LiDAR two hours after sunrise in central London, UK (Barlow et al., 2011); and wind profiler measurements were 250–400 m for 2 days in summer in Nashville, USA (Angevine et al., 2003). However, investigation of the z_i profile for each day confirms z_{i0} is an important control on the start-up shape of the CBL profiles (not shown).
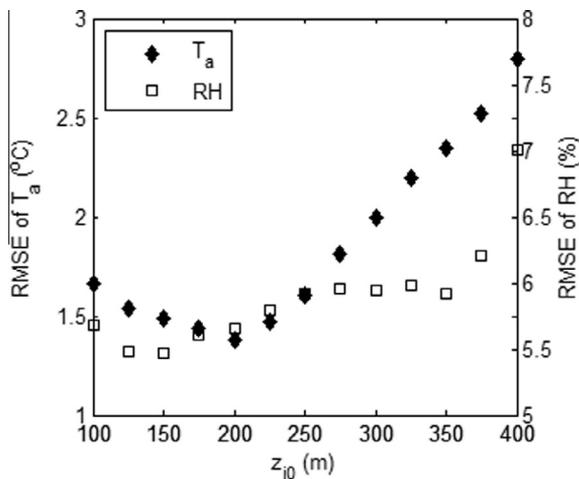

Fig. 10. Impact of changing initial convective boundary layer (z_{i0}) on modelled air temperature (T_a) and relative humidity (RH) using average initial vertical gradients of potential temperature and specific humidity for 6 days radiosonde measurements ($\partial\theta/\partial z$ = 0.043 K m^{-1} and $\partial q/\partial z$ = 0.009 g kg^{-1} m^{-1}): sensitivity test B3 (Table 3c) of BLUEWS.
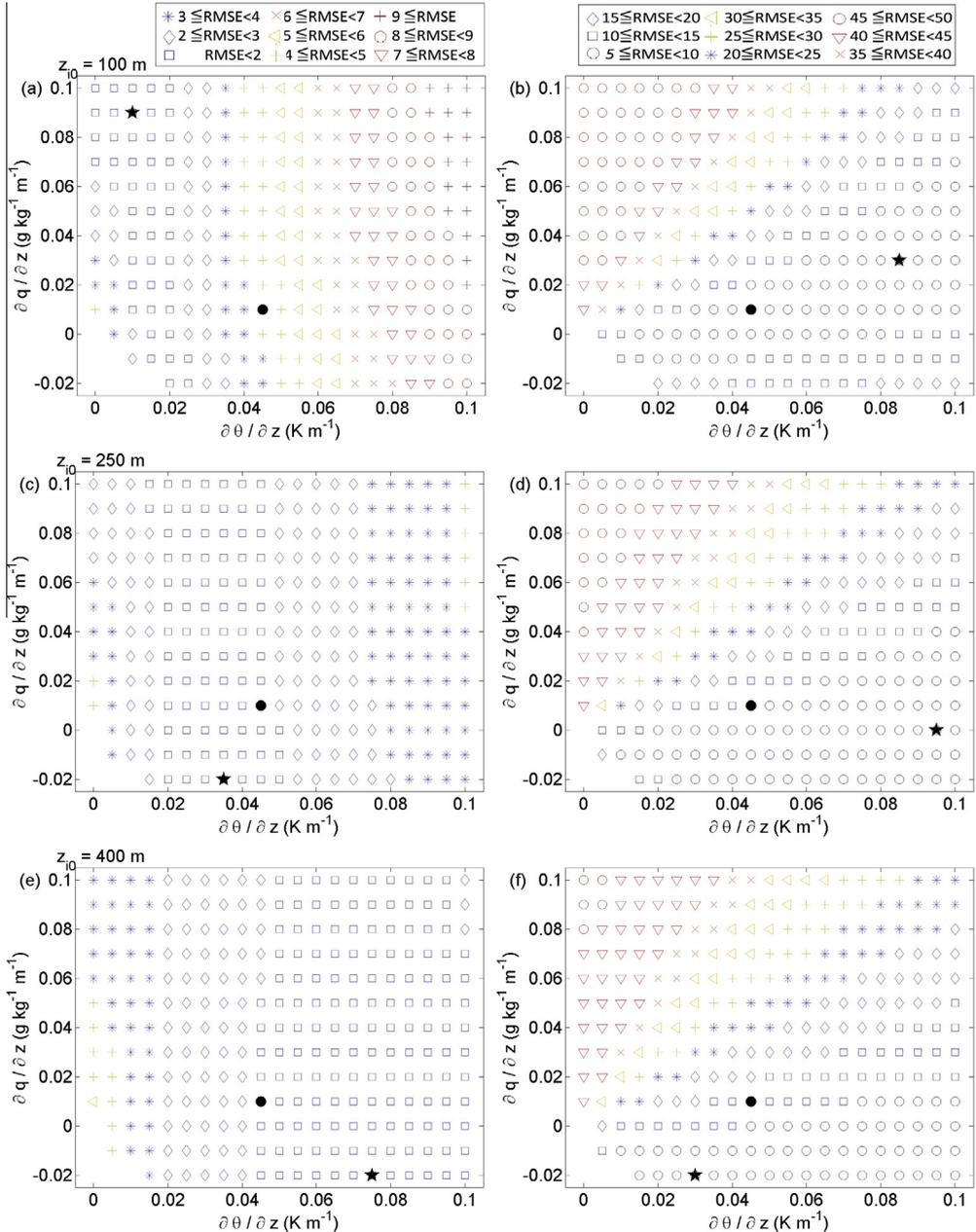
Fig. 11. Root Mean Square Error (*RMSE*) (left) air temperature (T_a), and (right) relative humidity (*RH*) for initial convective boundary layer (z_{i0}) (a, b) 100 m, (c, d) 250 m (e, f) 400 m for different combination of initial vertical gradients of potential temperature ($\partial\theta/\partial z$ on x-axis) and specific humidity ($\partial q/\partial z$ on y-axis): sensitivity test B4 (Table 3c) of BLUEWS. The closest point to average values of $\partial\theta/\partial z$ (=0.043 K m^{-1}) and $\partial q/\partial z$ (=0.009 g kg^{-1} m^{-1}) is indicated by a black dot ($\bullet$) and minimum *RMSE* by a star ($\star$).

To find the reasonable range of $\partial\theta/\partial z$ and $\partial q/\partial z$, and to investigate the combination which minimises *RMSE* of the modelled variables, different combinations of z_{i0}, $\partial\theta/\partial z$ and $\partial q/\partial z$ are shown for BLUEWS. Three heights are used for z_{i0}: 100, 250, or 400 m (Table 3c, B4). For each z_{i0}, $\partial\theta/\partial z$ is varied from 0 to 0.1 K m^{-1}, with 0.005 K m^{-1} increment steps, and $\partial q/\partial z$ is varied from -0.02 to 0.1 g kg^{-1} m^{-1} with 0.01 g kg^{-1} m^{-1} increment steps. Thus 819 combinations are tested in total. The *RMSE* of T_a and *RH* for each combination of z_{i0}, $\partial\theta/\partial z$ and $\partial q/\partial z$ are plotted in Fig. 11. The closest point to average values of $\partial\theta/\partial z$ (=0.043 K m^{-1}) and $\partial q/\partial z$ (=0.009 g kg^{-1} m^{-1}), and the minimum *RMSE* point, are indicated with a black point and a star, respectively. For all z_{i0}, the combination which gives the minimum *RMSE* (star) is not similar to the average (point) values of $\partial\theta/\partial z$ and $\partial q/\partial z$, but the *RMSE* is similar, except for T_a when z_{i0} = 100 m (Fig. 11a). T_a is more sensitive to $\partial\theta/\partial z$ and $\partial q/\partial z$ when z_{i0} is smaller (Fig. 11a, c, and e). For example, a $\partial\theta/\partial z$ larger than 0.05 K m^{-1} generates a *RMSE* greater than 5 °C for the T_a. This can be explained by thermodynamic processes of the CBL model; $\partial\theta/\partial z$ and $\partial q/\partial z$ determine the heat fluxes into the CBL by entrainment and the contribution of heat fluxes to changing T_a is larger with a shallower CBL. With smaller z_{i0}, $\partial\theta/\partial z$ affects T_a more than $\partial q/\partial z$ (Fig. 11a). The *RMSE* of *RH* apparently increases with smaller $\partial\theta/\partial z$ and larger $\partial q/\partial z$ for all z_{i0}. Focusing on a particular combination of $\partial\theta/\partial z$ and $\partial q/\partial z$, the *RMSE* of *RH* tends to be larger when z_{i0} is smaller (Fig. 11b, d, and f), which can be explained in the same way as T_a in terms of thermodynamic processes. The *RMSE* of *RH* is very large for some combinations of $\partial\theta/\partial z$ and $\partial q/\partial z$ if the application is to estimate T_{mrt}, but the error remains negligible as the *RH* impact to T_{mrt} is minimal (Fig. 7).
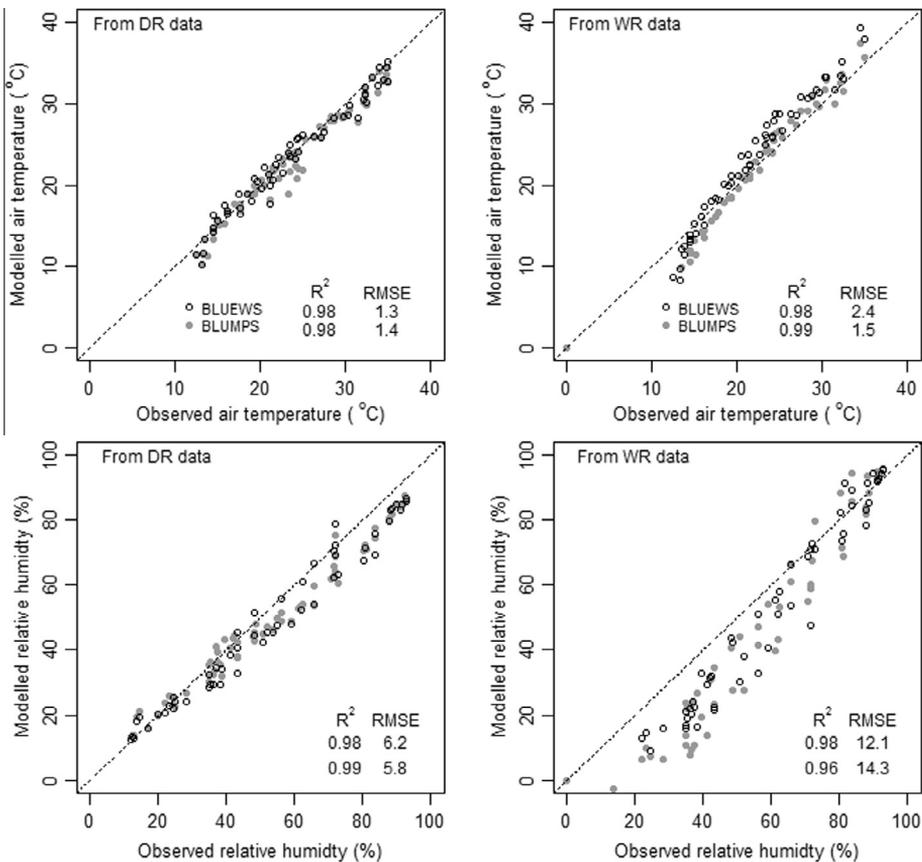

Fig. 12. Modelled and observed (upper) air temperature (T_a) and (lower) relative humidity (*RH*) for suburban site in Sacramento using observed data at (left) DR and (right) WR.

Consequently, when the initial values are selected for the coupled models to be applied to the T_{mrt} estimation, z_{i0} can be taken from the generally observed range of 100–400 m, but using some combinations of $\partial\theta/\partial z$ and $\partial q/\partial z$ with small z_{i0}, e.g. 100 m will cause a large error in T_a. Given a threshold of *RMSE* of T_a less than 4 °C, when z_{i0} is more than 250 m, $\partial\theta/\partial z$ and $\partial q/\partial z$ can be taken from most of the range of measured values at Sacramento. With the smaller z_{i0}, e.g. 100 m shown in this analysis, T_a is more sensitive to $\partial\theta/\partial z$. To obtain an accuracy of T_a below the threshold, $\partial\theta/\partial z$ needs to have a value less than 0.035 K m^{-1} for whole range of $\partial q/\partial z$.

6. Application to modelling of urban air temperature and relative humidity

BLUEWS and BLUMPS allow urban air temperature and relative humidity at the local-scale to be calculated from those measured at meteorological stations located elsewhere (non-urban or other urban areas), and allow prognostic values to be obtained. Here the DR and WR air temperature and relative humidity values are perturbed prior to calculating the SU values (with Section 4 settings). Thus, the results include two land cover differences (DR, WR) associated with the meteorological measurements relative to the meteorological information needed.

Fig. 12 shows that the modelled T_a and *RH* have good correlations with the observation at SU. However, *RMSE* of T_a = 1.3 (1.4) °C and *RMSE* of *RH* = 6.2 (5.8)% for BLUEWS (BLUMPS) when DR data are used, and *RMSE* of T_a = 2.4 (1.5) °C and *RMSE* of *RH* = 12.1 (14.3)% when WR data are used. The former underestimates T_a (Fig. 13), while the latter overestimates (Fig. 14). It is assumed that the measurements that the model is being evaluated against are representative of their upwind fetch. The current runs used static surface characteristics, rather than taking into account the dynamic changes in the probable source area characteristics of the SU observations.

The model has been applied with one, rather than multiple steps between the two points of interest. In reality the atmosphere blows downwind (so not necessarily between the two points of interest) and the upwind conditions of the site of interest may differ (Fig 3). Model improvement may be obtained by using a sequence of steps or using a 3-D modelling approach. However both would
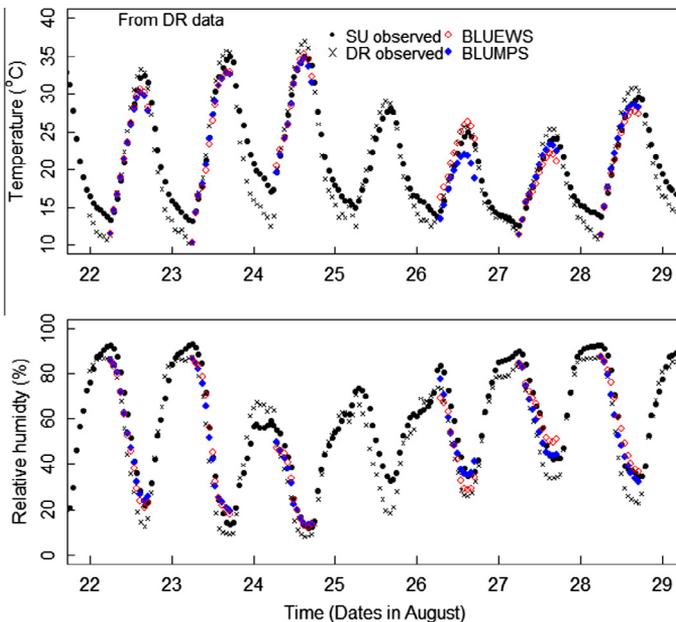

Fig. 13. Suburban (SU) (upper) air temperature and (lower) relative humidity modelled from dry rural (DR) data using coupled models (BLUEWS/BLUMPS) in comparison with the observation at suburban and dry rural sites.
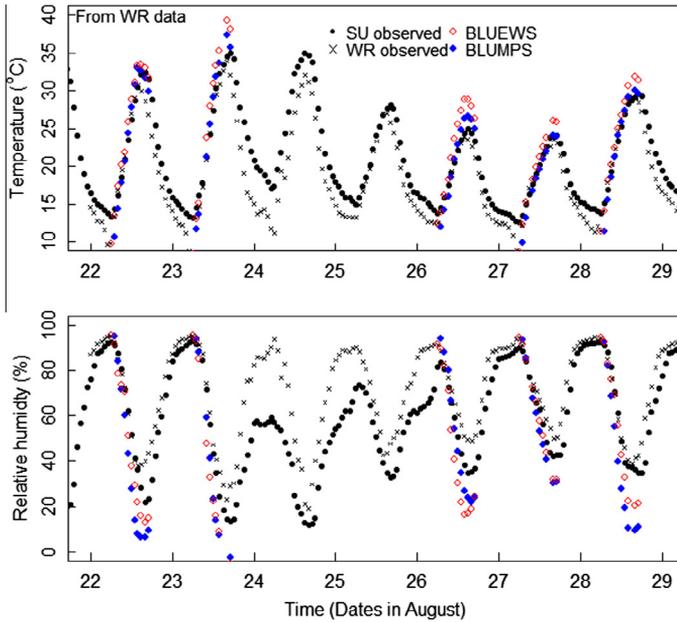
Fig. 14. As Fig. 13 but with WR data.

significantly enhance the modelling complexity and require considerable more information about the surface and initial state conditions and for 3-D modelling the atmospheric boundary conditions.

As seen in Figs. 13 and 14, observed T_a and RH are different between SU and rural sites during the daytime, which can systematically cause an error in the modelled T_{mrt}. For instance, the WR observed T_a is 0.46 °C lower than the SU observed T_a on average daytime and using the WR data roughly causes 2.1 °C underestimation of T_{mrt} at SU, which is calculated by using the results of the SOLWEIG sensitivity test (Section 5.1). The BLUEWS/BLUMPS modelled variables are estimated for the local-scale, so the SOLWEIG air temperature and humidity are modified with the environmental lapse rate (0.0064 K m^{-1}) to bring them to the level of interest. Alternatively, the additional resistance between the local and micro-scale could be used; however, this requires wind data to be transferred. This information is not currently needed within SOLWEIG. This new system showcases the potential to improve the modelling of T_{mrt} by using meteorological variables more representative of urban areas instead of using the data from non-urban sites. The SU modelled T_a is 0.36 °C higher than the WR observed T_a on average during the daytime and results in a 1.7 °C higher T_{mrt} than the WR used. These results show that the coupled models can provide more site-specific input data to the T_{mrt} modelling.

7. Conclusions

The coupled convective boundary layer and land surface models (BLUEWS/BLUMPS) provide daytime meteorological variables appropriate for outdoor thermal comfort estimations. The evaluation undertaken here uses observations from radiosonde releases plus three micrometeorological sites (suburban, irrigated sod-farm and extensive unirrigated grassland) in Sacramento, to assess boundary layer height ($RMSE_{BLUEWS,SU}$ = 86 m), potential temperature ($RMSE_{BLUEWS,SU}$ = 1.5 °C), specific humidity ($RMSE_{BLUEWS,SU}$ = 1.0 g kg^{-1}), sensible ($RMSE_{BLUEWS,SU}$ = 59 W m^{-2}) and latent heat fluxes ($RMSE_{BLUEWS,SU}$ = 42 W m^{-2}). The coupled model provides estimates for turbulent heat fluxes as good as the offline versions (SUEWS/LUMPS). The coupled results are similar, but the more biophysically based BLUEWS performs better for specific humidity even though not for latent heat flux.

Sensitivity tests of initial values at sunrise (CBL height, vertical gradients of potential temperature and specific humidity at CBL height) indicate that initial CBL height has a small impact on air temperature and relative humidity. However, combined with the required vertical gradients of potential temperature and specific humidity at lower initial heights (e.g. 100 m), large errors may occur. If an initial height of more than 250 m is used, the BLUEWS modelled air temperature and relative humidity are insensitive to the vertical gradients. Use of the observations to adjust the vertical gradients at each time step by profile (i.e. radiosonde) data improves model performance.

The ability of BLUEWS to use rural data to simulate suburban air temperature and relative humidity is better for a dry grassland area than a heavily irrigated area (*RMSE* = 1.3 °C, 6%; 2.4 °C, 12%, respectively). Sensitivity tests of the mean radiant temperature calculations demonstrate that air temperature is more critical than relative humidity (for SOLWEIG). Use of the modelled air temperature and relative humidity for the suburban land surface would improve the mean radiant temperature results from using the rural only data.

With the boundary layer growth model only applicable to daytime convective conditions, further developments are needed. Although fixed boundary layer heights could be specified, the inclusion of a nocturnal boundary layer height algorithm related to meteorological conditions will aid continuous dynamic modelling of air temperature and relative humidity as well as improving the estimation of nocturnal outdoor thermal comfort. Explicit coupling between BLUEWS/ BLUMPS and the micro-scale urban radiation model (SOLWEIG) is planned. The model presented here, has the advantage of insignificant computer resources compared to more complex models. The rapid computational time also has the potential to improve initial conditions for more computationally intense models.

Acknowledgements

Appendix A.

Variable	Unit	Description
α	–	Parameter for turbulent heat fluxes within LUMPS
$\alpha_{building}$	–	Effective surface albedo of buildings
$\alpha_{conifer}$	–	Effective surface albedo of coniferous trees
$\alpha_{deciduous}$	–	Effective surface albedo of deciduous trees
α_{grass}	–	Effective surface albedo of grass
$\alpha_{pavement}$	–	Effective surface albedo of pavement
α_{water}	–	Effective surface albedo of water
β	$W\,m^{-2}$	Parameter for turbulent heat fluxes within LUMPS
θ	K	Potential air temperature
θ_0	K	Initial potential temperature
θ_+	K	Potential temperature just above the CBL
θ_v	K	Virtual potential temperature
ρ	$kg\,m^{-3}$	Density of air
$\triangle\theta_v$	K	Virtual potential temperature difference across the capping inversion

Appendix A. (continued)

Variable	Unit	Description
$\triangle Q_s$	W m^{-2}	Storage heat flux
$\partial\theta/\partial z$	K m^{-1}	Vertical gradient of potential temperature at the top of CBL
$\partial q/\partial z$	g kg^{-1} m^{-1}	Vertical gradient of specific humidity at the top of CBL
a_i (i = 1, 2, 3)	–	Regression coefficients for OHM
b_i (i = 1, 2)	–	Constants used in the Tennekes and Driedonks (1981) entrainment scheme
$A_{surface}$	ha	The surface area of the study grid
BLUEWS	–	**CBL** model + **SUEWS**
BLUMPS	–	**CBL** model + **LUMPS**
CBL	–	Convective boundary layer
C_p	J kg^{-1} K^{-1}	Specific heat capacity at constant pressure
DoY	–	Day of year
DR	–	Dry rural site
$f_{auto\ irrigation}$	–	Plan area fraction of irrigated surface using automatic irrigation
$f_{building}$	–	Plan area fraction of buildings
$f_{coniferous\ vegetation}$	–	Plan area fraction of coniferous vegetation
$f_{deciduous\ vegetation}$	–	Plan area fraction of deciduous vegetation
$f_{irrigated\ grass}$	–	Plan area fraction of irrigated grass
$f_{pavement}$	–	Plan area fraction of pavement
f_{soil}	–	Plan area fraction of bare soil without rocks
$f_{unirrigated\ grass}$	–	Plan area fraction of unirrigated grass
f_{water}	–	Plan area fraction of water
g	m s^{-2}	Gravitational acceleration
I_e	mm h^{-1}	External piped water use or irrigation
$K\downarrow$	W m^{-2}	Incoming short-wave radiation
$K\downarrow_{rep}$	W m^{-2}	Incoming short-wave radiation replaced with average values
$L\downarrow$	W m^{-2}	Incoming long-wave radiation
L_v	J g^{-1}	Latent heat of vaporization
LUMPS	–	Local scale Urban Meteorological Parameterization Scheme
OHM	–	Objective Hysteresis Model
q	g kg^{-1}	Specific humidity
q_0	g kg^{-1}	Initial specific humidity
q_+	g kg^{-1}	Specific humidity just above convective boundary layer
Q^*	W m^{-2}	Net all-wave radiation
Q_H	W m^{-2}	Sensible heat flux
Q_E	W m^{-2}	Latent heat flux
Q_F	W m^{-2}	Anthropogenic heat flux
RH	%	Relative humidity
$RH_{(DR\rightarrow DR)}$	%	Modelled relative humidity for DR using initial input data from DR (Section 6)
$RH_{(DR\rightarrow SU)}$	%	Modelled relative humidity for SU using initial input data from DR (Section 6)
$RH_{(obs\_DR)}$	%	Observed relative humidity at DR (Section 6)
$RH_{(SU)}$	%	Modelled relative humidity for SU from data at DR/WR (Section 6)
RMSE	–	Root mean square error
R^2	–	The coefficient of determination
SOLWEIG	–	Solar and Long Wave Environmental Irradiance Geometry-model

Appendix A. (*continued*)

Variable	Unit	Description
SU	–	Suburban site
SUEWS	–	Surface Urban Energy and Water balance Scheme
t	s	Time
T_a	°C	Air temperature
T_{mrt}	°C	Mean radiant temperature
$T_{a(DR \to DR)}$	°C	Modelled temperature for DR using initial input data from DR (Section 6)
$T_{a(DR \to SU)}$	°C	Modelled temperature for SU using initial input data from DR (Section 6)
$T_{a(obs\_DR)}$	°C	Observed temperature at DR (Section 6)
$T_{a(SU)}$	°C	Modelled temperature from data at DR/ WR (Section 6)
T_H	°C	Maximum air temperature limit in Eq. (17) of Järvi et al. (2011)
T_L	°C	Minimum air temperature limit in Eq. (17) of Järvi et al. (2011)
u	m s^{-1}	Horizontal wind speed
u_*	m s^{-1}	Friction velocity
ULSM	–	Urban land surface model
w_*	m s^{-1}	Convective velocity
w_s	m s^{-1}	Subsidence velocity
WR	–	Wet rural site
z_{0m}	m	Roughness length for momentum
z_{0v}	m	Roughness length for heat and water vapour
z_d	m	Zero displacement height
z_h	m	Mean building height
z_{hv}	m	Mean vegetation height
z_i	m	Boundary layer height
z_{i0}	m	Initial boundary layer height

References

Anandakumar, K., 1999. A study on the partition of net radiation into heat fluxes on a dry asphalt surface. Atmos. Environ. 33, 3911–3918.

Angevine, W.M., White, A.B., Senff, C.J., Trainer, M., Banta, R.M., Ayoub, M.A., 2003. Urban–rural contrasts in mixing height and cloudiness over Nashville in 1999. J. Geophys. Res. 108, 1–10. AAC 3.

ASHRAE, 2001. ASHRAE Fundamentals Handbook 2001 (SI Edition) American Society of Heating, Refrigerating, and Air-Conditioning Engineers, ISBN: 1883413885.

Barlow, J.F., Dunbar, T.M., Nemitz, E.G., Wood, C.R., Gallagher, M.W., Davies, F., O'Connor, E., Harrison, R.M., 2011. Boundary layer dynamics over London, UK, as observed using Doppler lidar during REPARTEE-II. Atmos. Chem. Phys. 11, 2111–2125.

Best, M.J., Grimmond, C.S.B., 2013. Analysis of the seasonal cycle within the first international urban land-surface model comparison. Bound. Layer Meteor. 146, 421–446.

Bueno, B., Norford, L., Hidalgo, J., Pigeon, G., 2013. The urban weather generator. J. Bldg. Perf. Sim. 6, 269–281.

Bueno, B., Hidalgo, J., Pigeon, G., Norford, L., Masson, V., 2012. Calculation of air temperatures above the urban canopy layer from measurements at a rural operational weather station. J. Appl. Meteor. Climatol. 52, 472–483.

Cleugh, H.A., Grimmond, C.S.B., 2001. Modelling regional scale surface energy exchanges and CBL growth in a heterogeneous, urban–rural landscape. Bound. Layer Meteor 98, 1–31.

de Bruin, H.A.R., Holtslag, A.A.M., 1982. A simple parameterization of the surface fluxes of sensible and latent-heat during daytime compared with the penman-monteith concept. J. Appl. Meteor. 21, 1610–1621.

Doll, D., Ching, J.K.S., Kaneshiro, J., 1985. Parameterization of subsurface heating for soil and concrete using net radiation data. Bound. Layer Meteor. 32, 351–372.

Dyer, A.J., 1974. A review of flux-profile relationships. Bound. Layer Meteor. 7, 363–372.

ERA-interim: The European Centre for Medium-range Weather Forecasts (ECMWF). Available online at http://data-portal.ecmwf.int/data/d/interim_daily/.

Erell, E., Williamson, T., 2006. Simulating air temperature in an urban street canyon in all weather conditions using measured data at a reference meteorological station. Int. J. Climatol. 26, 1671–1694.

Flagg, D.D., Taylor, P.A., 2011. Sensitivity of mesoscale model urban boundary layer meteorology to the scale of urban representation. Atmos. Chem. Phys. 11, 2951–2972.

Fuchs, M., Hadas, A., 1972. The heat flux density in a non-homogeneous bare loessial soil. Bound. Layer Meteor. 3, 191–200.

Grimmond, C.S.B., 1992. The suburban energy balance meteorological considerations and results for a midlatitude west-coast city under winter and spring conditions. Int. J. Climatol. 12, 481–497.

Grimmond, C.S.B., Oke, T.R., 1991. An evaporation–interception model for urban areas. Water Resour. Res. 27, 1739–1755.

Grimmond, C.S.B., Cleugh, H.A., 1994. A simple method to determine obukhov lengths for suburban areas. J. Appl. Meteor. 33, 435–440.

Grimmond, C.S.B., Oke, T.R., 1995. Comparison of heat fluxes from summertime observations in the suburbs of four north American cities. J. Appl. Meteor. 34, 873–889.

Grimmond, C.S.B., Oke, T.R., 1999a. Evapotranspiration rates in urban areas. Impacts of Urban Growth on Surface Water and Groundwater Quality, Birmingham, International Association of Hydrological Sciences Publication 259, 235–243.

Grimmond, C.S.B., Oke, T.R., 1999b. Aerodynamic properties of urban areas derived from analysis of surface form. J. Appl. Meteor. 38, 1262–1292.

Grimmond, C.S.B., Oke, T.R., 1999c. Heat storage in urban areas: Local-scale observations and evaluation of a simple model. J. Appl. Meteor. 38, 922–940.

Grimmond, C.S.B., Oke, T.R., 2002. Turbulent heat fluxes in urban areas: Observations and a local-scale urban meteorological parameterization scheme (LUMPS). J. Appl. Meteor. 41, 792–810.

Grimmond, C.S.B., Cleugh, H.A., Oke, T.R., 1991. An objective urban heat-storage model and its comparison with other schemes. Atmos. Environ. 25, 311–326.

Grimmond, C.S.B., Oke, T.R., Cleugh, H.A., 1993. The role of rural in comparisons of observed suburban–rural flux differences. Exchange processes at the land surface for a range of space and time scales, Yokohama, International Association of Hydrological Sciences Publication 212, 165–174.

Hanna, S., Chang, J., 1992. Boundary-layer parameterizations for applied dispersion modeling over urban areas. Bound. Layer Meteor. 58, 229–259.

Högström, U., 1988. Non-dimensional wind and temperature profiles in the atmospheric surface layer: a re-evaluation. Bound. Layer Meteor. 42, 55–78.

IPCC, 2012. Summary for policymakers. In: Field, C.B., Barros, V., Stocker, T.F., Qin, D., Dokken, D.J., Ebi, K.L., Mastrandrea, M.D., Mach, K.J., Plattner, G.-K., Allen, S.K., Tignor, M., Midgley, P.M. (Eds.), Managing the Risks of Extreme Events and Disasters to Advance Climate Change Adaptation, A Special Report of Working Groups 1 and 2 of the Intergovernmental Panel on Climate Change. Cambridge University Press, Cambridge, UK and New York, USA, pp. 3–21.

Järvi, L., Grimmond, C.S.B., Christen, A., 2011. The Surface Urban Energy and Water Balance Scheme (SUEWS): evaluation in Los Angeles and Vancouver. J. Hydrol. 411, 219–237.

Järvi, L., Grimmond, C.S.B., Onomura, S., 2014. SUEWS Manual: Version 2014a. Available online at http://londonclimate.info.

Kawai, T., Ridwan, M.K., Kanda, M., 2009. Evaluation of the simple urban energy balance model using selected data from 1-yr flux observations at two cities. J. Appl. Meteor. Climatol. 48, 693–715.

Landsat, 10th August 2006: USGS, Accessed 23-01-2014.

Lindberg, F., Grimmond, C.S.B., 2011a. Nature of vegetation and building morphology characteristics across a city: influence on shadow patterns and mean radiant temperatures in London. Urban Ecosyst. 14, 617–634.

Lindberg, F., Grimmond, C.S.B., 2011b. The influence of vegetation and building morphology on shadow patterns and mean radiant temperatures in urban areas: model development and evaluation. Theor. Appl. Climatol. 105, 311–323.

Lindberg, F., Holmer, B., Thorsson, S., 2008. SOLWEIG 1.0 – modelling spatial variations of 3D radiant fluxes and mean radiant temperature in complex urban settings. Int. J. Biometeorol. 52, 697–713.

Lindberg, F., Holmer, B., Thorsson, S., Rayner, D., 2013. Characteristics of the mean radiant temperature in high latitude cities—implications for sensitive climate planning applications. Int. J. Biometeorol. 58, 613–627.

Loridan, T., F. Lindberg, O. Jorba, S. Kotthaus, S. Grossman-Clarke, and C. S. B. Grimmond, 2013: High resolution simulation of the variability of surface energy balance fluxes across central London with urban zones for energy partitioning. Bound.-Layer Meteor., 147, 493–523.

Loridan, T., Grimmond, C.S.B., Offerle, B.D., Young, D.T., Smith, T.E.L., Järvi, L., Lindberg, F., 2010. Local-Scale Urban Meteorological Parameterization Scheme (LUMPS): Longwave radiation parameterization and seasonality-related developments. J. Appl. Meteor. Climatol. 50, 185–202.

Macdonald, R.W., Griffiths, R.F., Hall, D.J., 1998. An improved method for the estimation of surface roughness of obstacle arrays. Atmos. Environ. 32, 1857–1864.

Masson, V., 2000. A physically-based scheme for the urban energy budget in atmospheric models. Bound. Layer Meteor. 94, 357–397.

Matzarakis, A., Rutz, F., Mayer, H., 2010. Modelling radiation fluxes in simple and complex environments: basics of the RayMan model. Int. J. Biometeorol. 54, 131–139.

Mayer, H., Höppe, P., 1987. Thermal comfort of man in different urban environments. Theor. Appl. Climatol. 38, 43–49.

McMichael, A.J., Woodruff, R.E., Hales, S., 2006. Climate change and human health: present and future risks. The Lancet 367, 859–869.

McNaughton, K.G., Spriggs, T.W., 1986. A mixed-layer model for regional evaporation. Bound. Layer Meteor. 34, 243–262.

Meyn, S.K., Oke, T.R., 2009. Heat fluxes through roofs and their relevance to estimates of urban heat storage. Energy Build. 41, 745–752.

Miao, S., Chen, F., LeMone, M.A., Tewari, M., Li, Q., Wang, Y., 2009. An observational and modeling study of characteristics of urban heat island and boundary layer structures in Beijing. J. Appl. Meteor. Climatol. 48, 484–501.

NREL, 2012. National Solar Radiation Data Base: Sacramento Metropolitan AP, CA (Class II). Available online at http://rredc.nrel.gov/solar/old_data/nsrdb/1991-2005/hourly/siteonthefly.cgi?id=724839. Accessed 2012-08-02.

NWP: Satellite Application Facility for Numerical Weather Prediction (NMP SAF). Available online at http://research.metoffice.gov.uk/research/interproj/nwpsaf/.

Offerle, B., Grimmond, C.S.B., Oke, T.R., 2003. Parameterization of net all-wave radiation for urban areas. J. Appl. Meteor. 42, 1157–1173.

Oke, T.R., 1987. Boundary layer climates, second ed. Routledge, London and New York, 12 and 281 pp..

Oke, T.R., 1988. The urban energy-balance. *Prog. Phys. Geograp.* 12, 471–508.

Pascal, M., Laaidi, K., Ledrans, M., Baffert, E., Caserio-Schönemann, C., Tertre, A., Manach, J., Medina, S., Rudant, J., Empereur-Bissonnet, P., 2006. France's heat health watch warning system. Int. J. Biometeorol. 50, 144–153.

Raupach, M.R., 2000. Equilibrium evaporation and the convective boundary layer. Bound. Layer Meteor. 96, 107–142.

Rayner, K.N., Watson, I.D., 1991. Operational prediction of daytime mixed layer heights for dispersion modelling. Atmos. Environ. 25, 1427–1436.

Souch, C., Grimmond, C.S.B., Wolfe, C.P., 1998. Evapotranspiration rates from wetlands with different disturbance histories: Indiana Dunes National Lakeshore. Wetlands 18, 216–229.

Stewart, I.D., Oke, T.R., Krayenhoff, E.S., 2013. Evaluation of the 'local climate zone' scheme using temperature observations and model simulations. Int. J. Climatol. 34, 1062–1080.

Swaid, H., Hoffman, M.E., 1990. Prediction of urban air temperature variations using the analytical CTTC model. Energy Build. 14, 313–324.

Tennekes, H., 1973. A model for the dynamics of the inversion above a convective boundary layer. J. Atmos. Sci. 30, 558–567.

Tennekes, H., Driedonks, A.G.M., 1981. Basic entrainment equations for the atmospheric boundary layer. Bound. Layer Meteor. 20, 515–531.

Van Ulden, A.P., Holtslag, A.A.M., 1985. Estimation of atmospheric boundary layer parameters for diffusion applications. J. Climate Appl. Meteor. 24, 1196–1207.